This manuscript was accepted by J. Chem. Phys. Click here to see the version of record.

# Simulations of grain boundaries between ordered hard sphere monolayer domains: orientation-dependent stiffness and its correlation with grain coarsening dynamics

Ziwei Guo (郭子威) and James T. Kindt[a)]

*Department of Chemistry, Emory University, Atlanta, Georgia 30322, USA*

**Abstract:**

The properties of grain boundaries (GBs) between ordered 2-d domains of a hard-sphere monolayer have been investigated using grand canonical Monte Carlo simulations. The capillary fluctuation method was used to determine the GB stiffness over a range of pressures, misorientations and inclinations. Stiffness was found to be sensitive to misorientation (mismatch in the orientation angle of neighboring grains), but not to depend on inclination (angle between the boundary and the grain orientation). Excess area per GB length was observed to follow the same trend as stiffness with respect to grain misorientation and GB inclination angles. Dynamical studies of the evolution of bicrystalline or multicrystalline monolayers with simple geometries show that the calculated angle-dependent stiffnesses correlate well with the rate at which the evolving grain structure decreases the lengths of various GB, in agreement with recent experimental results on monolayers of colloidal microspheres.

## 1. Introduction:

Grain boundaries (GBs), the interfaces between neighboring crystal domains that are similar in structure but differ in orientation, are very important in the study of physical properties of polycrystal materials such as metals, ceramics, semi-conductors[1-3]. Material strength, grain growth, phase transformations, recrystallization and electrical conductivity are highly related to the GB[4-8]. Therefore, controlling the GB plays a vital role in manipulation of the mechanical, optical and electrical properties of polycrystalline materials[9]. GB can be characterized by two key parameters: the grain-boundary stiffness Γ and the interface mobility $M$, which govern the structure and dynamics of curvature-driven grain-growth[10]. Stiffness Γ is the sum of the interfacial line tension $\gamma$ and its second derivative with respect to GB orientation $\gamma''$. Geometrically, the GB can be

a) jkindt@emory.edu

This manuscript was accepted by J. Chem. Phys. Click here to see the version of record.

characterized by two angles: (i) "misorientation", which is the difference in orientation between the two neighboring crystal grains, and (ii) "inclination", which is the orientation of the GB line.[11] (The inclination is defined as the smaller orientation difference between the GB and the two grain domains it divides.) Various methods have been developed to study the GB stiffness and mobility in experiments[10, 12-14] and simulations[15-18].

Colloidal polycrystalline monolayers have been shown to be useful model systems to study GB and grain growth[19]. Various experiments take advantage of the large size (~μm) and slow dynamics (~s), which make it possible to follow the behavior directly by optical microscopy[20, 21]. Hexagonal polycrystalline monolayers can be prepared by confining spherical colloidal particles through gravity onto a liquid[22] or solid surface[14] or confined to a gap between surfaces[23]. Under appropriate conditions, the interactions between particles will be dominated by short-ranged repulsions so that the colloids can be modeled as hard spheres.[24] In the limit where fluctuations normal to the plane can be neglected, monodisperse hard spheres become isomorphic to the two-dimensional system of hard disks (HD).[25]

In the present study we will assume that this fully 2-d limit is reached, as is appropriate for sufficiently large and heavy colloidal particles.[24] While we will continue to refer to "spheres" to emphasize the relevance to experimental colloidal systems, we will take also advantage of the extensive simulation literature on HD phase behavior. It has been shown[26, 27] that the HD phase diagram features a first-order phase coexistence between a fluid phase at area fraction $\eta = 0.700$ and hexatic phase at $\eta = 0.716$. The hexatic phase is stable over a narrow range of area fractions, and undergoes a continuous transition to a 2-d solid phase upon further compression to $\eta \approx 0.720$.[27] The grains modeled here fall in the range of area fractions from $\eta = 0.727$ to 0.782 and so can be considered 2-d solids.

Although stiffness of GB in colloidal monolayers has been addressed through several experiments,[10, 14, 23] no systematic study has been done to show the dependence of stiffness on misorientation, inclination and pressure. By engineering the grain domains in our simulations, we are able to study the GB systematically with controllable parameters. In this study, stiffness dependence on these variables will be reported for monolayers of uniform hard sphere, and compared with experimental observations[10, 14]. Simulations are performed in the grand canonical ensemble, implemented here using the solvent-repacking Monte Carlo (SRMC)[28] algorithm to aid in particle exchange in the dense system. Setting a common chemical potential facilitates

This manuscript was accepted by J. Chem. Phys. Click here to see the version of record.

comparison across systems under varying geometries at the same pressure. Local particle insertion and removal moves, distributed across many processors in parallel through domain decomposition, allow the local density at the boundary and within the grains to reach equilibrium and undergo fluctuations independently, rather than relying on uniform expansion and compression of the whole system to achieve constant pressure. Fluctuations of the GB shape are interpreted via the capillary fluctuation method (CFM)[29] to yield the stiffness.

This article will first report calculations of the stiffness of boundaries between adjacent domains of hard spheres in the 2-d solid phase, with attention to effects of pressure, grain misorientation, and GB inclination. In the second section, the pre-melting behaviors of GB at pressures approaching the melting transition, and a non-equilibrium faceting behavior observed at high pressures, will be discussed qualitatively. Finally, dynamic Monte Carlo studies of simple 2- and 4-grain systems are used to show how the evolution of grain sizes and shapes are influenced by grain misorientation in manner that is qualitatively consistent with the trends in GB stiffness.

## 2. Methods:

### A. System Construction and initialization

In the study of stiffness, ordered grains of spheres are set up in a pair of parallel stripes making two parallel GBs align with the $x$ direction. Initial ordered structures were taken from equilibrated 2-d ordered phases generated in previous studies[28]. For simulations at the highest chemical potential / pressure conditions, the starting structure was a perfect hexagonal lattice with density close to the expected equilibrium density. The use of parallel stripe grains with boundaries that are continuous via periodic boundaries provide a well-defined misorientation between the grains, a fixed mean inclination between the boundary and the grains, and a fixed GB length. The two domains have the same area in the initial configuration, and are separated by a distance of $\sigma$ in the $y$ direction to remove particle overlaps. This gap between the grains is filled quickly by the SRMC algorithm.

In the dynamic study, the two (or four) domains with different orientations are engineered to the desired domain shapes. A distance of $\sigma$ between domains is applied for the same reason to prevent overlapping. The output configuration after 1000 MC cycles in grand canonical ensemble is used as the initial configuration for the dynamic study in NVT ensemble, in which the gaps are already filled while the areas of domains do not change significantly.

**B. Solvent-Repacking Monte Carlo**

To sample over the grand canonical ensemble at some particle fugacity $f = \exp(\beta\mu)$ at high packing density, the solvent-repacking Monte Carlo (SRMC) algorithm was used and is described here briefly. The SRMC method uses configurational bias Monte Carlo[30] (CBMC) strategy to generate a set of positions for a set of particles to replace the particles present in a circular cavity randomly selected within the simulation box. After defining the cavity and selecting its radius (as a random value between 1 and 1.4 $\sigma$ in the present case), a number $k$ of insertion moves will be performed to randomly and uniformly sample the cavity region in each cycle $i$. The $j'$th particle will then be selected with a probability:

$$P_{i,j'} = \frac{\exp(-\beta u'_{i,j'})}{\sum_{j=1}^{k} \exp(-\beta u'_{i,j'})} = \frac{\exp(-\beta u'_{i,j'})}{W'_i} \tag{1}$$

where $u'_{i,j'}$ is the auxiliary potential (the logarithm of the radial distribution function (RDF) for hard spheres with an area fraction 0.69 is used in this work; this and choices for $k$ were consistent with previous work[28]) for the interaction of the $j'$th particle with particles inserted in previous cycle and the solvent shell around the cavity. The insertion cycle will be repeated until some predetermined conditions are met: either particle number in cavity reach a maximum (20 in this work) or none of the $k$ trial positions are successful. We thus can get a maximum number of particles $n_{max}$ that can be inserted in this cavity region (which is independent of the current number.)

The probability for selecting a configuration with number of particles $i'$ is:

$$P(i') = \frac{\omega_{i'}}{\sum_{i=0}^{n_{max}} \omega_i} \tag{2}$$

where the weight $\omega_{i'}$ associating the configurations with different numbers of particles can be calculated as:

$$\omega_i = \frac{f^i}{\Lambda^{di}} \frac{{v_{cav}}^i}{i! \prod_{i'=1}^{i} k_{i'}} W'_i \frac{\exp(-\beta U_i)}{\exp(-\beta U'_i)} \tag{3}$$

where $\Lambda$ is the de Broglie thermal wavelength (set to 1 in all simulations); $d$ is the dimension of the system; $U_i$ and $U'_i$ are the true potential energy (always equal to zero) and the auxiliary bias potential energy, respectively. Calculation of weights associated with the current configuration of particles involves the generating of alternative "dummy" trial positions, as is standard in CBMC.

This manuscript was accepted by J. Chem. Phys. Click here to see the version of record.

The overall acceptance probability for transition from current state with $n_{cav}$ particles in cavity to the new state with $n_{cav'}$ particles can be written as:

$$acc_{n_{cav}\to n_{cav'}} = min\left[1, \frac{\sum_{i=0}^{n_{max,new}} \omega_{i,new}}{\sum_{i=0}^{n_{max,current}} \omega_{i,current}}\right] \quad (4)$$

## C. Order parameter and GB detection

Bond-orientational order parameter[31] $\Psi_6$ is used to characterize the local crystalline order of particle $j$:

$$\Psi_6(\vec{r}_j) = \frac{1}{N_j}\sum_{k=1}^{N_j} e^{i6\Delta\theta_{jk}} \quad (5)$$

where $\Delta\theta_{jk}$ is defined as the angle between the $x$ direction with the vector connecting the central particle $j$ and one of its $N_j$ nearest neighbor $k$ within a cutoff $1.5\sigma$. The orientation of the hexagon formed by six neighbors of particle $j$ can then be calculated by $\theta_6 = \arg(\Psi_6)/6$, which is a value varied from 0 to 60° due to the symmetry of hexagon. The orientation of the grain domain can be quantified by averaging all the $\theta_6$ of particles belonging to the domain. In the rest of this report, $\theta_6$ refers to the orientation of the domain instead of single particle for simplicity.

To detect the variation in the position of the two GB's along the $x$ dimension, we divide the simulation box into a 100×100 grid. Multiple tests showed this granularity is fine enough, and that the use of smaller grid squares does not affect the stiffness calculated. The average of the $\theta_6$ for particles in each grid and the four nearest grid squares of the same $x$ coordinate is measured to represent the orientation of each grid square. (Averaging over several grid squares in the $y$ direction serves to smooth over noise associated with local pockets of disorder, whether at the boundary or elsewhere, which otherwise lead to false indications of the GB location.) The height $h$ of the grain boundary is taken as the $y$ coordinate of the "edge point" grid square, defined as the grid square with $\theta_6$ closest to the mean of the $\theta_6$ values of the two grains. The GB is represented by connecting "edge points" all together (Fig. 1).

This manuscript was accepted by J. Chem. Phys. Click here to see the version of record.

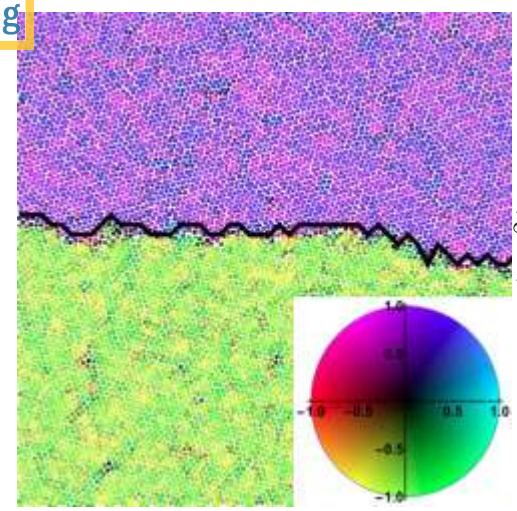

FIG. 1. Snapshot of a hard-sphere monolayer at fugacity $1\times10^7$ with the GBs presented in a 200 $\sigma$ ×200 $\sigma$ box (only one GB in a region $100\sigma\times100\sigma$ is shown here for clarity). The spheres are color-coded by order parameter $\Psi_6$ represented by the color shown in the inset. The x and y axis represent the real and imaginary part of $\Psi_6$, respectively.

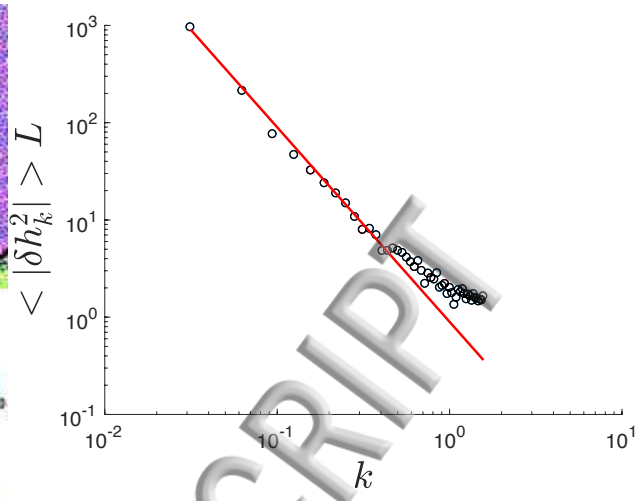


FIG. 2. F.T. spectrum of the fluctuation of GB at fugacity $f$=$1.0\times10^7$ in a $200\sigma\times200\sigma$ box. Red line is the linear fit of the spectrum data (circle points) with slope fixed at -2.

### D. Capillary Fluctuation Method

The capillary fluctuation method is commonly used to relate the wavelength-dependent fluctuation of the interface to the interfacial free energy or stiffness in a variety of contexts [10, 16, 32, 33]. GBs in each frame during the simulation are represented by the method discussed above, which can be described by a function of the distance along the $x$ direction and frame $t$: $h(x,t)$. To correct for drift or diffusion of the GB over the course of the simulation we use fluctuations relative to the current mean position of the GB: $\delta h(x,t) = h(x,t) - \langle h(t)\rangle_x$. For each frame, the following Fourier Transform (F.T.) can be written:

$$\delta h(k) = \frac{1}{L}\int_0^L \delta h(x)\exp(-ikx)\,dx \tag{6}$$

Each frame's spatial fluctuation $\delta h(x)$ is transformed using Eq. 6 into $\delta h(k)$, which is the intensity of the mode with wave number $k$ in Fourier Spectrum, where $k = 2\pi m/L$ ($m = 0, \pm1, \pm2, ...$) and $L$ is the length of GB. $\langle|\delta h(k)|^2\rangle$ is calculated as an average over all frames, and is related to the stiffness Γ of the GB by CFM[29]:

$$\log(\langle|\delta h(k)|^2\rangle L) = -2\log(k) + \log(\frac{k_B T}{\Gamma}) \tag{7}$$

This manuscript was accepted by J. Chem. Phys. Click here to see the version of record.

In practice, a linear fitting of Eq. (7) with a fixed slope –2 is performed to fit the F.T. spectrum to find stiffness Γ from the $y$-intercept (Fig. 2). We found in general that the power spectrum of fluctuations deviated upward from the low-$k$ trend at high $k$ (i.e. short wavelength). The CFM is derived from continuum theory and so is not expected to fit fluctuations with high $k$. The apparent crossover to a different high-$k$ regime was dependent on the system, but excluding points with $|m|$ higher than 15 (corresponding to $k > 0.5\ \sigma^{-1}$, or wavelengths $< 12\ \sigma$) from the linear fitting produced satisfactory results in all cases. Why the continuum model breaks down at such a large wavelength (as opposed to a wavelength of ~1-2 $\sigma$ where the discrete particulate nature of the interface becomes unavoidable) is not clear, but the explanation may lie in the disorder local to the GB and the accompanying uncertainty in defining the boundary positions.

**E. Implementation details**

A domain-decomposition scheme is used to parallelize the simulations. The system (with a box size $200\sigma\times200\sigma$ or $300\sigma\times300\sigma$ in stiffness calculation, $200\sigma\times200\sigma$ or $250\sigma\times250\sigma$ in dynamic study) was divided into an 8×8 or 12×12 grid with a randomly selected origin. In each MC cycle, a predetermined number of MC move attempts were performed independently within each grid square on separate processors, with no addition, removal, or translation of particles within a zone of distance of $0.5\sigma$ from domain borders. For GCMC simulation of GB fluctuations, each MC cycle contains 1000 SRMC move attempts followed by 2000 regular translation move attempts (max. displacement of $0.05\sigma$) performed in each grid square. After every MC cycle, a new origin for the grid was chosen and particles are redistributed among processors so that the border regions are constantly changing. To sample GB fluctuations $\delta h(x)$, the equilibration and production periods consisted of at least 5000 and 20000 MC cycles, respectively, within the grand canonical ensemble.

In studies of the evolution of 2- and 4-grain systems, an equilibration period of 1000 MC cycles as defined above was used to allow the GB to relax from their initial straight arrangements and to allow the ordered grains to reach a steady density.

Dynamic MC studies were performed under canonical ensemble conditions (at constant $N$ and $A$). At least 3000 MC cycles are run, with 20000 regular translation moves per domain in each cycle.

This manuscript was accepted by J. Chem. Phys. Click here to see the version of record.

Reduced units, scaled to the particle diameter $\sigma$ and the thermal energy $k_BT$ are used throughout. The pressure $P^*$ (in units of $k_BT/\sigma^2$) was calculated using the radial distribution at contact[34]:

$$P^* = \rho + \frac{\pi}{2}\rho^2 g(1_+) \quad (8)$$

with $\rho = N/A$. The radial distribution at contact is obtained by fitting the pair distance histograms to a third-order polynomial out to 1.05 times the contact length. Area fraction $\eta$ is calculated as to $\pi\rho/4$, corresponding to the projected area of non-overlapping spheres on a flat surface or the area coverage of discs of unit area. The bulk area fraction is measured using the average number density within the grains' interiors.

## 3. Results and discussion:

The first part of this section demonstrates the systematic measurement of stiffness under various conditions including box size, pressure (varied through changing particle chemical potential), misorientation and inclination. Enthalpic and entropic contributions to the stiffness will be discussed. The second part focuses on a phenomenon we noticed from our simulation: GB buckling or faceting during a gradual increase in the system pressure. The apparent origins of this phenomenon and implications for simulation approaches and the behavior of experimental systems under compression will be discussed. The last section presents the results of dynamic studies that test how the stiffness of GB correlate with the dependence of grain growth rates on orientational factors.

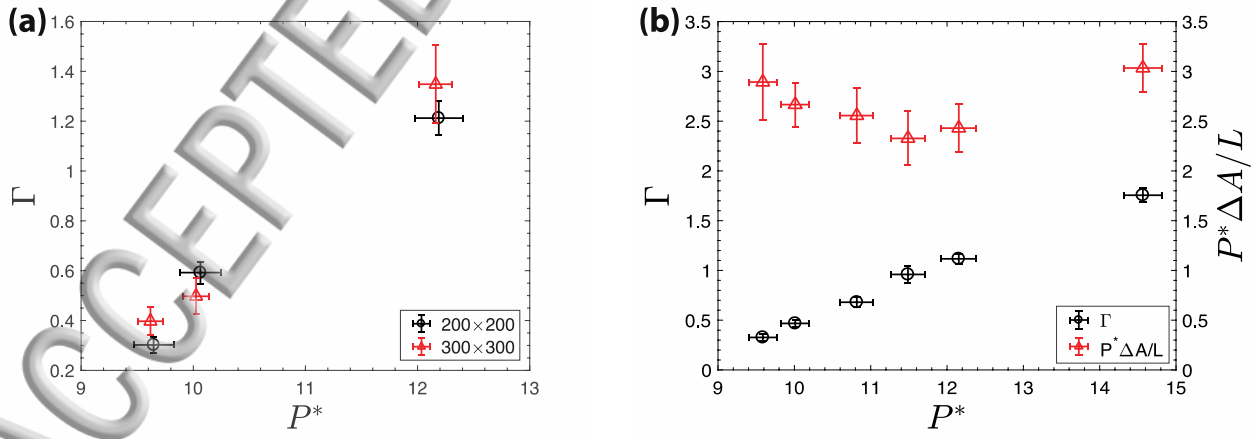


FIG. 3. Stiffness dependence on (a) system size with fixed GB misorientation 27.4° and inclination 11.1°; (b) pressure with fixed system size $200\sigma\times200\sigma$, misorientation 30° and inclination 15°. The product of pressure with excess surface area per unit length of GB ($P\Delta A/L$) is also shown in (b).

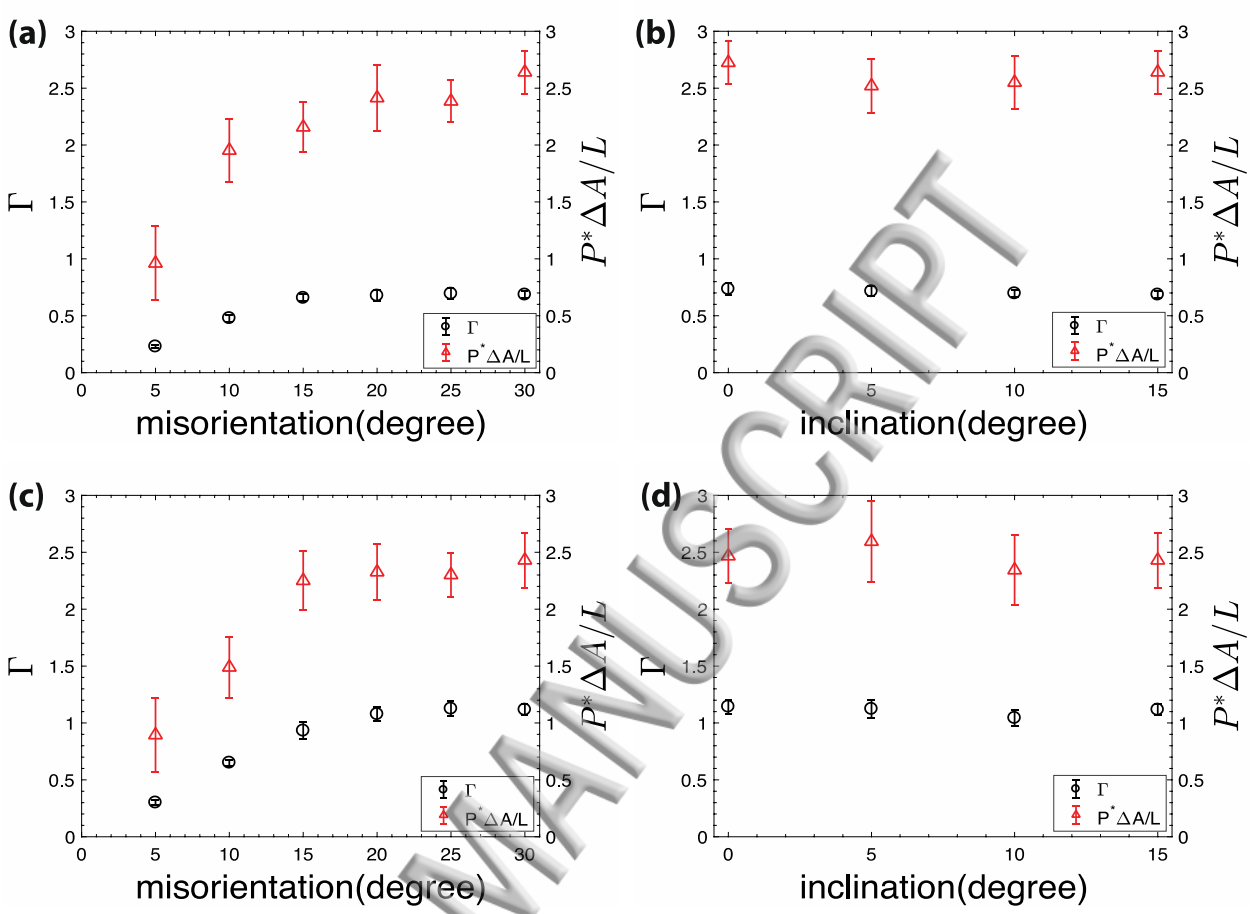


FIG. 4. Stiffness and excess interfacial enthalpy per unit length of GB ($P^*\Delta A/L$) from simulations at system size $200\sigma\times200\sigma$ on (a) misorientation with and inclination 15° at fugacity $2.0\times10^6$; (b) inclination with fixed misorientation 30° at fugacity $2.0\times10^6$; (c) misorientation with inclination 15° at fugacity $1.0\times10^7$; (d) inclination with misorientation 30° at fugacity $1.0\times10^7$.



### A. Stiffness and line tension

We first studied the stiffness dependence on system size. In principle, system size should not affect the GB. Practically, GB may suffer from the finite size effect in simulations. Simulations at $100\sigma\times100\sigma$ were tested but were not pursued because the drift in GB positions would sometimes bring them close enough together for a grain to fuse with its periodic image. We compared results of simulations under three pressures with different system size ($200\sigma\times200\sigma$ or $300\sigma\times300\sigma$), keeping misorientation and inclination the same (Fig. 3(a)). No significant difference is observed. The increase in computational expense to equilibrate the fluctuations with increasing box length $L$ is expected to scale as $L^3$, as the number of particles scales with $L^2$ while the relaxation time of the

This manuscript was accepted by J. Chem. Phys. Click here to see the version of record.

longest-wavelength mode scales with $L$.[16] Therefore, for efficiency and to allow better convergence, all following simulations are performed with a box size $200\sigma \times 200\sigma$ (except one case in *Section. C* which required a larger box size). Although this range of box sizes is not wide enough to rule out the possibility of finite-size effects, the general agreement at these system sizes, the absence of a systematic size-dependent trend in the calculated stiffness, and considerations of efficiency and statistical sampling led us to adopt a box size $200\sigma \times 200\sigma$ for all further stiffness calculations. The stiffness dependence on pressure is studied with a fixed misorientation and inclination (Fig. 3(b) and Table. I). A linear relation is observed. A GB stiffness has been evaluated as $1.7\times10^{-15}$ J m$^{-1}$ from experimental images of a fluctuating GB in a system of 2.7 $\mu$m colloidal particles[10] at a number density of 0.11 $\mu m^{-2}$. Upon conversion to reduced units ($k_BT/\sigma$) this corresponds to $\Gamma$= 1.1, in good qualitative agreement with the present simulation results. We hesitate to examine the agreement in stiffness values between experiment and simulation more closely, because of the difficulty in calibrating the state of the experimental system onto the simulation conditions with sufficient precision.

Fig. 4(a) and (b) shows the stiffness dependence on misorientation and inclination. A higher stiffness is observed as the misorientation increases. Stiffness and enthalpy show the same dependence on misorientation. No significant dependence on inclination is seen in either the stiffness or the enthalpy of the grain boundary. These results are consistent with a recent experimental study of the dynamics of 2-d colloidal grain growth,[14] which showed boundaries between neighboring grains with large misorientations disappeared faster than low-misorientation boundaries, but that the probability distribution of GB was uniform and unchanging with respect to inclination angle. From this we may conclude that the second derivative of GB free energy with respect to angle of inclination must be small, and that therefore the line tension can be assumed equal to the stiffness to a very good approximation.

Given that the stiffness extracted from simulation can be treated as a line tension (excess free energy per unit length), it is instructive to analyze the components of that free energy. Since the potential energy of the HS system is zero for all allowable configurations and the kinetic energy per particle is only a function of temperature, the excess internal energy of the GB is zero. The excess enthalpy $\Delta H$ for this 2-d system in reduced units is therefore $P^*\Delta A$, with $\Delta A$ the excess area (the area difference in area between a uniform system and a system with the same number of particles having a GB). The excess entropy associated with the GB at constant surface pressure is

This manuscript was accepted by J. Chem. Phys. Click here to see the version of record.

Therefore $T\Delta S = P^*\Delta A - \Delta G$, and so the excess entropy per unit length of the GB is $\Delta S/L = (P^*\Delta A/L - \Gamma)$. The red symbols in Fig. 3(b) and 4 show the product of pressure $P^*$ with excess surface area $\Delta A$ per unit length $L$ of the GB. The difference between the red symbols and $\Gamma$ reflects the excess interfacial entropy per unit length, which decreases with increasing pressure to about $P^*$=12 and then levels off. The dependences of enthalpy on GB misorientation and inclination at constant fugacity (Fig. 4(c) and 4(d)) track the corresponding dependences of stiffness on these properties.

As pressure is decreased toward the melting pressure, the excess area per unit length associated with the boundary increases significantly (from about 0.2 σ to about 0.3 σ.) This is caused by the interface widening as it turns into a locally liquid region, an example of pre-melting as has been observed at grain boundaries in a variety of polycrystalline systems[35-37]. In fact, the presence of a wide and fluctuating pre-melted zone made it impossible to evaluate the position of the interface at pressures below 9.5 $k_BT/\sigma^2$.

Pre-melting to a fluid layer of width $w$ is expected to be spontaneous when the line tension between the two solid grains is greater than the combination of the combined fluid-solid interfacial tensions of the two solid-fluid interfaces formed[35], plus a bulk contribution (which vanishes at the transition pressure) that is proportional to $w$. The fluid-solid interfacial tension is not easily obtained since the 2-d solid and fluid phases do not coexist at equilibrium. Instead we consider the experimentally derived interfacial stiffness values reported by Thorneywork *et al.*[24] for the fluid-hexatic interface at coexistence at an inclination 15°. Converted into reduced units, this gives an estimate for the fluid-solid interfacial tension of $\Gamma = 0.085$. When we use the data in Figure 3(b) to extrapolate our stiffness dependence to the transition pressure ($P^*$=9.18), we find the corresponding stiffness ($\Gamma$ = 0.235) to be higher than twice this estimate, consistent with the observed pre-melting at the GB.



TABLE. I . Physical properties of systems at different pressures, with misorientation 30° and inclination 15° in a $200\sigma \times 200\sigma$ simulation box. Area fraction listed is taken from grain interiors.

This manuscript was accepted by J. Chem. Phys. Click here to see the version of record.

| fugacity | $P^*$ | area fraction $\eta$ | $\Gamma$ |
|---|---|---|---|
| $6 \times 10^5$ | 9.58±0.18 | 0.7269±2E-4 | 0.327±0.033 |
| $1 \times 10^6$ | 10.01±0.18 | 0.7341±3E-4 | 0.468±0.038 |
| $2 \times 10^6$ | 10.82±0.21 | 0.7456±1E-4 | 0.681±0.050 |
| $5 \times 10^6$ | 11.49±0.22 | 0.7539±2E-4 | 0.960±0.082 |
| $1 \times 10^7$ | 12.15±0.23 | 0.7611±2E-4 | 1.117±0.049 |
| $1 \times 10^8$ | 14.56±0.25 | 0.7825±9E-5 | 1.756±0.071 |

**B. GB buckling during dynamical pressure compression**

When we investigated the stiffness dependence on pressure, we noticed that equilibration of systems at high pressure $P^* = 14.56$ (corresponding to fugacity of $1.0 \times 10^8$) when starting from a lower area fraction ($\eta$=0.740) configuration tended to produce structures with buckled or faceted GB. An example is shown in Fig. 5. Upon extending the trajectory, this buckled structure might evolve but would not relax to a flat boundary within a reasonable time for simulation. The CFM analysis in such cases produced an amplitude spectrum that did not fit the $k^{-2}$ model well at all, because the assumption of sampling over amplitudes at all wavelengths was not met. The spontaneous adoption of facets could be the result of a strong dependence of interfacial free energy on the angle of inclination, in apparent contradiction to our findings above. In this case, however, the buckling occurred no matter the angle of inclination; setting up the ribbon with inclination at 0° still produced facets.

The buckling occurred during equilibration under GCMC conditions while the total number of particles in the simulation was increasing. To determine whether buckling was a by-product of this non-equilibrium process, we constructed an ideal, defect-free hexagonal domain with an area fraction close to the value at the desired pressure ($P^*$ =14.56). In this case, the buckling was not observed, and the CFM method yielded well-behaved results that were consistent in trends from lower pressure (shown in Fig. 3(b)). Starting with an ideal, defect-free domain at a lower area fraction, and allowing the density to increase via particle exchange at the higher fugacity, produced buckling. It can then be concluded that the GB buckling is related to the non-equilibrium process of increased densification of the grains at constant area through particle addition, which (through a mechanism that is unclear – not observably related to the creation or annihilation of specific dislocations) caused uneven stresses in the system that were relaxed through deformation of the

GB. A recent experimental study by Cash *et al*.[23] showed that formation of a locally melted region near a GB following a laser "blast" produced a deformation of the grain boundary in what may be a related phenomenon. It is conceivable that other experimental cases where particles continue to add to a polycrystalline ordered surface could produce a similar buckling effect on GB.

We have noticed that, compared with GCMC simulations in a square, monocrystalline, periodically repeating system, systems containing GB are much faster at the relaxation of total particle numbers and increasing local packing density in the 2-d ordered state. The apparent reason is that the GB can act as both a source and a sink of dislocations, allowing the lattice constant to shrink at constant box dimension via the addition of rows to the domain stripes. This is perhaps the flip side of an experimental observation by Deutschländer *et al*.[38], that polycrystalline 2-d systems quenched rapidly into melting conditions will generate defects preferentially near grain boundaries, which proceed inward to melt the ordered domains.

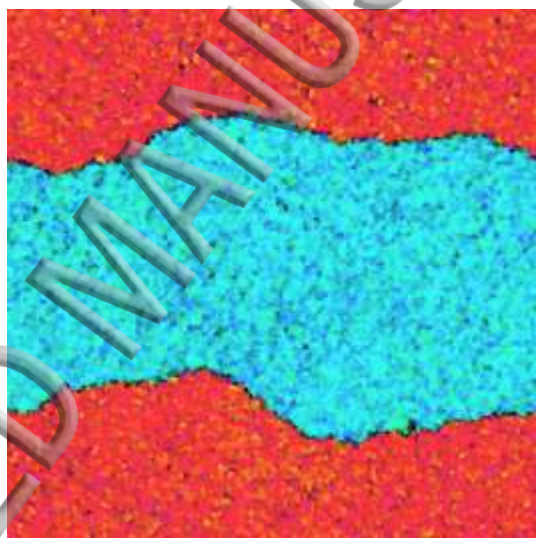

FIG. 5. Snapshots of the buckled configuration with GB misorientation at 30°and inclination 0° after 23000 MC moves in grand-canonical ensemble at fugacity $f = 1 \times 10^8$, initiated from a lower-density structure. This snapshot is color-coded by order parameter $\Psi_6$ as shown in Fig. 1.

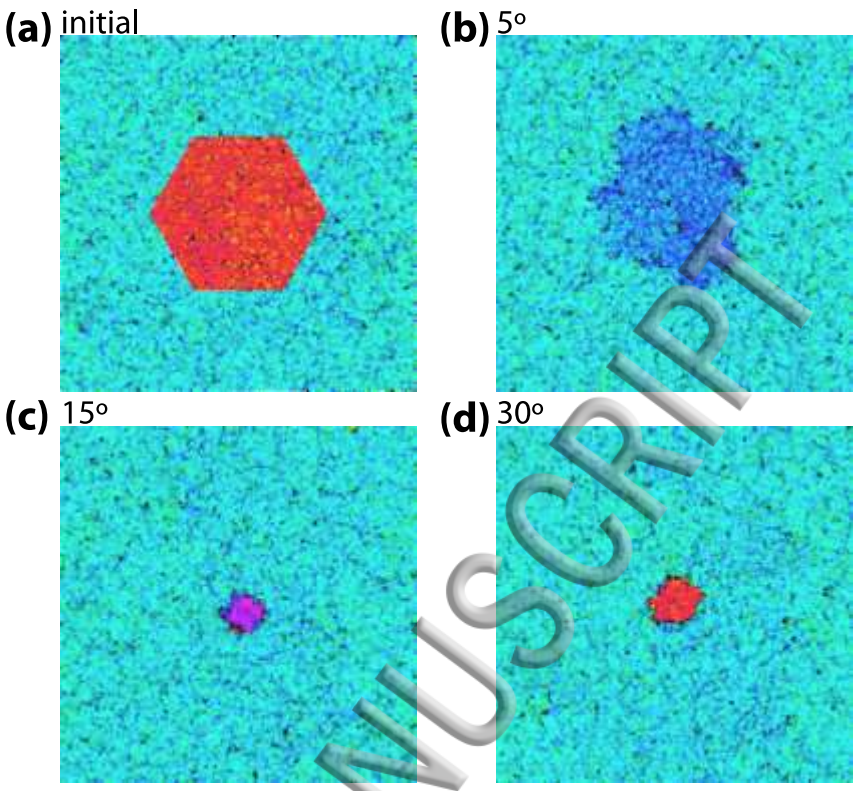


FIG. 6. (a) Starting arrangement shape of 2-grain system showing to indicate initial size and shape of misoriented domain; 30° misorientation shown. (b)-(d) Snapshots of the configuration after 7000 MC moves in grand-canonical ensembles for GB misorientation 5°, 15° and 30°. All snapshots are color-coded by order parameter $\Psi_6$ as shown in Fig. 1.

This manuscript was accepted by J. Chem. Phys. Click here to see the version of record.

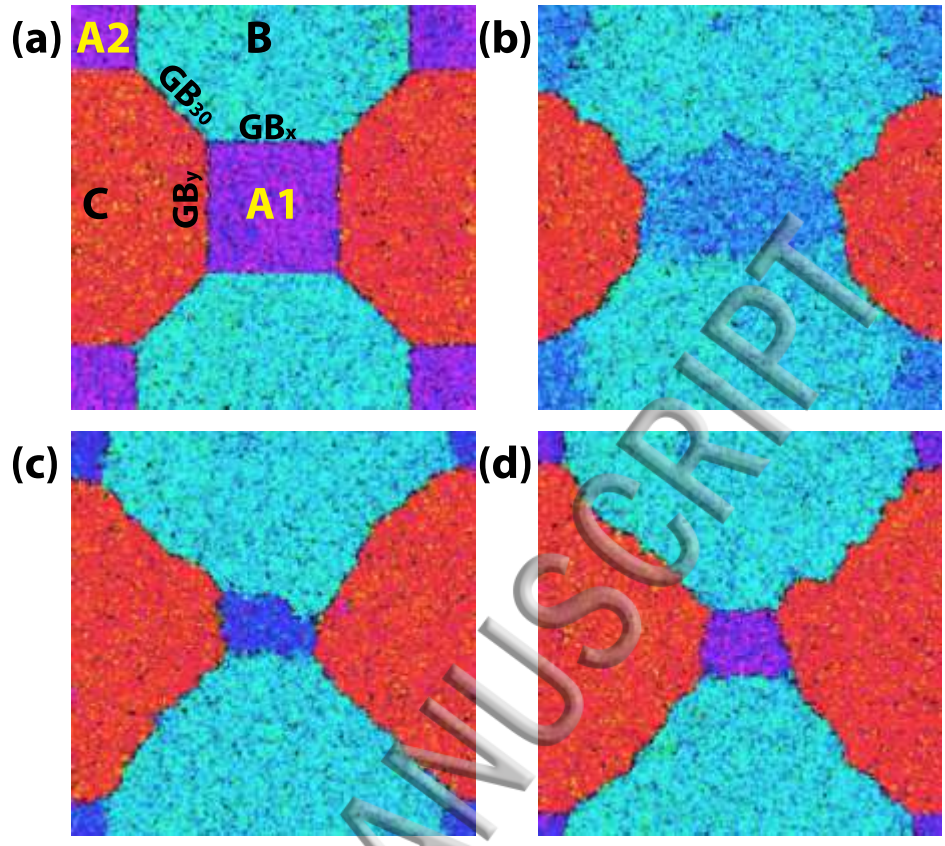


FIG. 7. (a) Snapshot of an initial configuration in a 4-grain system with misorientation 15° for both $GB_x$ and $GB_y$; Snapshots of the configuration after 40000 MC moves in constant-N ensemble in a 4-grain system with $GB_x$ misorientation (b) 5°; (c) 10° and (d) 15°. All snapshots are color-coded by order parameter $\Psi_6$ as shown in Fig. 1.

### C. Dynamics of grain coarsening

Although Monte Carlo simulation does not produce a trajectory that is directly related to a dynamic algorithm, the evolution of a MC trajectory that uses local displacement moves (as opposed to the unphysical SRMC moves that can incorporate changes in particle number and collective rearrangements) can give qualitative insight into dynamics. This is particularly true for colloidal systems where Brownian dynamics might be a good approximation.[39] To determine how the MC dynamics of grain coarsening are influenced by grain and GB orientations, we first modeled an isolated hexagonal domain at misorientations of 30°, 15°, and 5°. The system containing a hexagonal domain (with an edge length $50\sigma$) is constructed within a $200\sigma \times 200\sigma$ box (Fig. 6(a)). The six GBs in each system have the same inclination as well, due to the symmetry of the hexagon. After 1000 MC cycles under grand canonical simulation, the shapes of the original hexagon shape cannot be recognized due to the fluctuation of the GB. Fig. 6 shows the snapshots

This manuscript was accepted by J. Chem. Phys. Click here to see the version of record.

after 7000 MC cycles. The shrinking rate for the domain with misorientation 5° is much slower than other two systems, which shrink on similar timescales. Taken together with the results of Fig. 4(c), these observations suggest that the GB shrinking rate is correlated with stiffness, as $\Gamma(5°) < \Gamma(15°) \approx \Gamma(30°)$. Results obtained under constant-N ensemble simulation (not shown) are qualitatively similar. We also constructed the system containing a square domain (not shown) with the same area as the hexagonal domain, where GB at different direction will have different inclination. The result shows no apparent difference between the rates of shrinking in X and Y dimensions, confirming that the shrinking rates depend negligibly on inclination.

A more complex system containing tiled octagonal and square grains with three different orientations was constructed as shown in Fig. 7(a), to further study how misorientation affects the domain coarsening when triple junctions (TJ) are present. Varying the orientation of the square domain (A1, A2) enables us to compare the shrinking rates of GB with different misorientations ($GB_x$, $GB_y$) in the same domain. The octagonal grains B and C have fixed $\theta_6$ (0° and 30°, respectively) which fix the misorientation of $GB_{30}$ at 30°. A larger simulation box ($250\sigma \times 250\sigma$) is used so that $GB_{30}$ is not too short. Three cases are shown where the misorientation for $GB_x$ is 5°, 10° and 15° (denoted as MisX5, MisX10 and MisX15, respectively); the corresponding misorientation for $GB_y$ is then 25°, 20° and 15°, respectively.

The shrinking rates are much slower compared to the two-domain systems. One reason is that if the square domains maintain their shape as they shrink, the reduction in GB length of the square will be counterbalanced by the increase in the octagon/octagon GB length, so the driving force (if all line tensions are equal) is lower by a factor of $(1\text{-}2^{-1/2})$. Friction associated with the TJ motion may also contribute. The order of overall shrinking rate is MisX5 < MisX10 ≈ MisX15 (Fig. 7), which can still be explained by the sum of the stiffness of $GB_x$ and $GB_y$. After 40000 MC cycles, the central domain (A1) becomes roughly rectangular (Fig. 7(b) and 7(c)), with the more-misoriented GB shrinking faster, consistent with the increase in stiffness with misorientation angle. In the case of MisX5, the 5° $GB_x$ actually expands as domain C (along with the BC grain boundary) shrinks, again consistent with the stiffness predictions. The general behavior is in full agreement with the experimental results and explanations given by Lavergne *et al.*[14], who found that low-misorientation GB tended to grow at the expense of high-misorientation GB in polycrystalline systems, and observed isotropic distributions of GB inclination angles at all misorientations. In

concert with the CFM results presented earlier, these findings illustrate the influence of the thermodynamic property (line tension) on the dynamics.

## 4. Conclusions:

The stiffness of grain boundaries in a two-dimensional hard-sphere system at packing fractions above the freezing transition has been analyzed using the capillary fluctuation method and grand canonical Monte Carlo. Stiffness was found to increase linearly with pressure, to be sensitive to misorientation of the grains (increasing steadily up to ~15° and changing slightly at higher angles) and to be nearly insensitive to the inclination of the GB with respect to the domains. The insensitivity to inclination indicates that in this system, it is a good approximation to equate the observed stiffness with the thermodynamic line tension. The enthalpic contribution to the line tension arising from the excess area decreases at low pressures, reaches a minimum, and increases as the excess area of the GB apparently approaches its minimum. Dynamic simulations of 2- and 4-grain systems arranged in simple geometries demonstrate the relevance of these findings to misorientation effects on grain coarsening rates, and are fully consistent with recently published experiments of 2-d colloidal grain coarsening dynamics.[14] The current results could be useful in providing input parameters for mesoscale modeling of grain growth in these systems,[40-42] as well a foundation for further studies of impurity segregation at GB in bidisperse hard-sphere monolayers.[43]

**Acknowledgments:**

Support from the Emory University Research Committee is gratefully acknowledged. This work used the Extreme Science and Engineering Discovery Environment (XSEDE) Comet cluster at the San Diego Supercomputer Center, which is supported by National Science Foundation grant number ACI-1548562, allocation TG-MCB110144. This work also used the resources of the Cherry L. Emerson Center for Scientific Computation.

**References:**

[1] C. Herring, *chapter in The Physics of Powder Metallurgy, edited by WE Kingston* (McGraw-Hill Book Co., New York, 1951).

[2] J. Howe, *Interfaces in materials: atomic structure, thermodynamics and kinetics of solid-vapor, solid-liquid and solid-solid interfaces* (New York: Wiley, 1997).

[3] A. Rollett, F. Humphreys, G. S. Rohrer, and M. Hatherly, *Recrystallization and Related Annealing Phenomena* (Elsevier, 2004),

[4] M. A. Meyers, A. Mishra, and D. J. Benson, "Mechanical Properties of Nanocrystalline Materials" Progress in materials science **51**, 427 (2006).
[5] K. Kreuer, "Proton-Conducting Oxides" Annual Review of Materials Research **33**, 333 (2003).
[6] C. S. Ruiz-Vargas, H. L. Zhuang, P. Y. Huang, A. M. Van Der Zande, S. Garg, P. L. McEuen, D. A. Muller, R. G. Hennig, and J. Park, "Softened Elastic Response and Unzipping in Chemical Vapor Deposition Graphene Membranes" Nano letters **11**, 2259 (2011).
[7] H. Van Swygenhoven, "Grain Boundaries and Dislocations" Science **296**, 66 (2002).
[8] T. Zykova-Timan, R. E. Rozas, J. Horbach, and K. Binder, "Computer Simulation Studies of Finite-Size Broadening of Solid–Liquid Interfaces: From Hard Spheres to Nickel" Journal of Physics: Condensed Matter **21**, 464102 (2009).
[9] V. Randle, "Grain Boundary Engineering: An Overview after 25 Years" Materials science and technology **26**, 253 (2010).
[10] T. O. Skinner, D. G. Aarts, and R. P. Dullens, "Grain-Boundary Fluctuations in Two-Dimensional Colloidal Crystals" Physical review letters **105**, 168301 (2010).
[11] G. Gottstein, and L. S. Shvindlerman, *Grain Boundary Migration in Metals: Thermodynamics, Kinetics, Applications* (CRC press, 2009),
[12] N. Eustathopoulos, "Energetics of Solid/Liquid Interfaces of Metals and Alloys" International metals reviews **28**, 189 (1983).
[13] Y. Huang, and F. Humphreys, "Measurements of Grain Boundary Mobility During Recrystallization of a Single-Phase Aluminium Alloy" Acta Materialia **47**, 2259 (1999).
[14] F. A. Lavergne, D. G. Aarts, and R. P. Dullens, "Anomalous Grain Growth in a Polycrystalline Monolayer of Colloidal Hard Spheres" Physical Review X **7**, 041064 (2017).
[15] M. Asta, C. Beckermann, A. Karma, W. Kurz, R. Napolitano, M. Plapp, G. Purdy, M. Rappaz, and R. Trivedi, "Solidification Microstructures and Solid-State Parallels: Recent Developments, Future Directions" Acta Materialia **57**, 941 (2009).
[16] S. M. Foiles, and J. Hoyt, "Computation of Grain Boundary Stiffness and Mobility from Boundary Fluctuations" Acta Materialia **54**, 3351 (2006).
[17] Z. T. Trautt, M. Upmanyu, and A. Karma, "Interface Mobility from Interface Random Walk" Science **314**, 632 (2006).
[18] J. Hoyt, Z. Trautt, and M. Upmanyu, "Fluctuations in Molecular Dynamics Simulations" Mathematics and Computers in Simulation **80**, 1382 (2010).
[19] S. Gokhale, K. H. Nagamanasa, R. Ganapathy, and A. Sood, "Grain Growth and Grain Boundary Dynamics in Colloidal Polycrystals" Soft Matter **9**, 6634 (2013).
[20] V. Prasad, D. Semwogerere, and E. R. Weeks, "Confocal Microscopy of Colloids" Journal of Physics: Condensed Matter **19**, 113102 (2007).
[21] P. Schall, "Laser Diffraction Microscopy" Reports on Progress in Physics **72**, 076601 (2009).
[22] P. Dillmann, G. Maret, and P. Keim, "Polycrystalline Solidification in a Quenched 2d Colloidal System" Journal of Physics: Condensed Matter **20**, 404216 (2008).
[23] C. E. Cash, J. Wang, M. M. Martirossyan, B. K. Ludlow, A. E. Baptista, N. M. Brown, E. J. Weissler, J. Abacousnac, and S. J. Gerbode, "Local Melting Attracts Grain Boundaries in Colloidal Polycrystals" Physical review letters **120**, 018002 (2018).
[24] A. L. Thorneywork, J. L. Abbott, D. G. Aarts, and R. P. Dullens, "Two-Dimensional Melting of Colloidal Hard Spheres" Physical review letters **118**, 158001 (2017).

[25] W. Qi, A. P. Gantapara, and M. Dijkstra, "Two-Stage Melting Induced by Dislocations and Grain Boundaries in Monolayers of Hard Spheres" Soft Matter **10**, 5449 (2014).
[26] E. P. Bernard, and W. Krauth, "Two-Step Melting in Two Dimensions: First-Order Liquid-Hexatic Transition" Physical review letters **107**, 155704 (2011).
[27] M. Engel, J. A. Anderson, S. C. Glotzer, M. Isobe, E. P. Bernard, and W. Krauth, "Hard-Disk Equation of State: First-Order Liquid-Hexatic Transition in Two Dimensions with Three Simulation Methods" Physical Review E **87**, 042134 (2013).
[28] J. T. Kindt, "Grand Canonical Monte Carlo Using Solvent Repacking: Application to Phase Behavior of Hard Disk Mixtures" The Journal of chemical physics **143**, 124109 (2015).
[29] S. A. Safran, *Statistical Thermodynamics of Surfaces, Interfaces, and Membranes* (Perseus Books, 1994), Vol. 90,
[30] J. I. Siepmann, and D. Frenkel, "Configurational Bias Monte Carlo: A New Sampling Scheme for Flexible Chains" Molecular Physics **75**, 59 (1992).
[31] D. R. Nelson, *Defects and Geometry in Condensed Matter Physics* (Cambridge University Press, 2002),
[32] Y. Jiang, and J. T. Kindt, "Simulations of Edge Behavior in a Mixed-Lipid Bilayer: Fluctuation Analysis" The Journal of chemical physics **126**, 01B624 (2007).
[33] S. Katira, K. K. Mandadapu, S. Vaikuntanathan, B. Smit, and D. Chandler, "Pre-Transition Effects Mediate Forces of Assembly between Transmembrane Proteins" Elife **5**, (2016).
[34] D. G. Chae, F. H. Ree, and T. Ree, "Radial Distribution Functions and Equation of State of the Hard-Disk Fluid" The Journal of Chemical Physics **50**, 1581 (1969).
[35] J. Broughton, and G. Gilmer, "Thermodynamic Criteria for Grain-Boundary Melting: A Molecular-Dynamics Study" Physical review letters **56**, 2692 (1986).
[36] A. M. Alsayed, M. F. Islam, J. Zhang, P. J. Collings, and A. G. Yodh, "Premelting at Defects within Bulk Colloidal Crystals" Science **309**, 1207 (2005).
[37] P. Williams, and Y. Mishin, "Thermodynamics of Grain Boundary Premelting in Alloys. Ii. Atomistic Simulation" Acta Materialia **57**, 3786 (2009).
[38] S. Deutschländer, C. Boitard, G. Maret, and P. Keim, "Grain-Boundary-Induced Melting in Quenched Polycrystalline Monolayers" Physical Review E **92**, 060302 (2015).
[39] E. Sanz, and D. Marenduzzo, "Dynamic Monte Carlo Versus Brownian Dynamics: A Comparison for Self-Diffusion and Crystallization in Colloidal Fluids" The Journal of chemical physics **132**, 194102 (2010).
[40] S. G. Kim, D. I. Kim, W. T. Kim, and Y. B. Park, "Computer Simulations of Two-Dimensional and Three-Dimensional Ideal Grain Growth" Physical Review E **74**, 061605 (2006).
[41] J. Gruber, H. Miller, T. Hoffmann, G. Rohrer, and A. Rollett, "Misorientation Texture Development During Grain Growth. Part I: Simulation and Experiment" Acta Materialia **57**, 6102 (2009).
[42] L. Zhang, J. Han, Y. Xiang, and D. J. Srolovitz, "Equation of Motion for a Grain Boundary" Physical review letters **119**, 246101 (2017).
[43] F. o. A. Lavergne, S. Diana, D. G. Aarts, and R. P. Dullens, "Equilibrium Grain Boundary Segregation and Clustering of Impurities in Colloidal Polycrystalline Monolayers" Langmuir **32**, 12716 (2016).

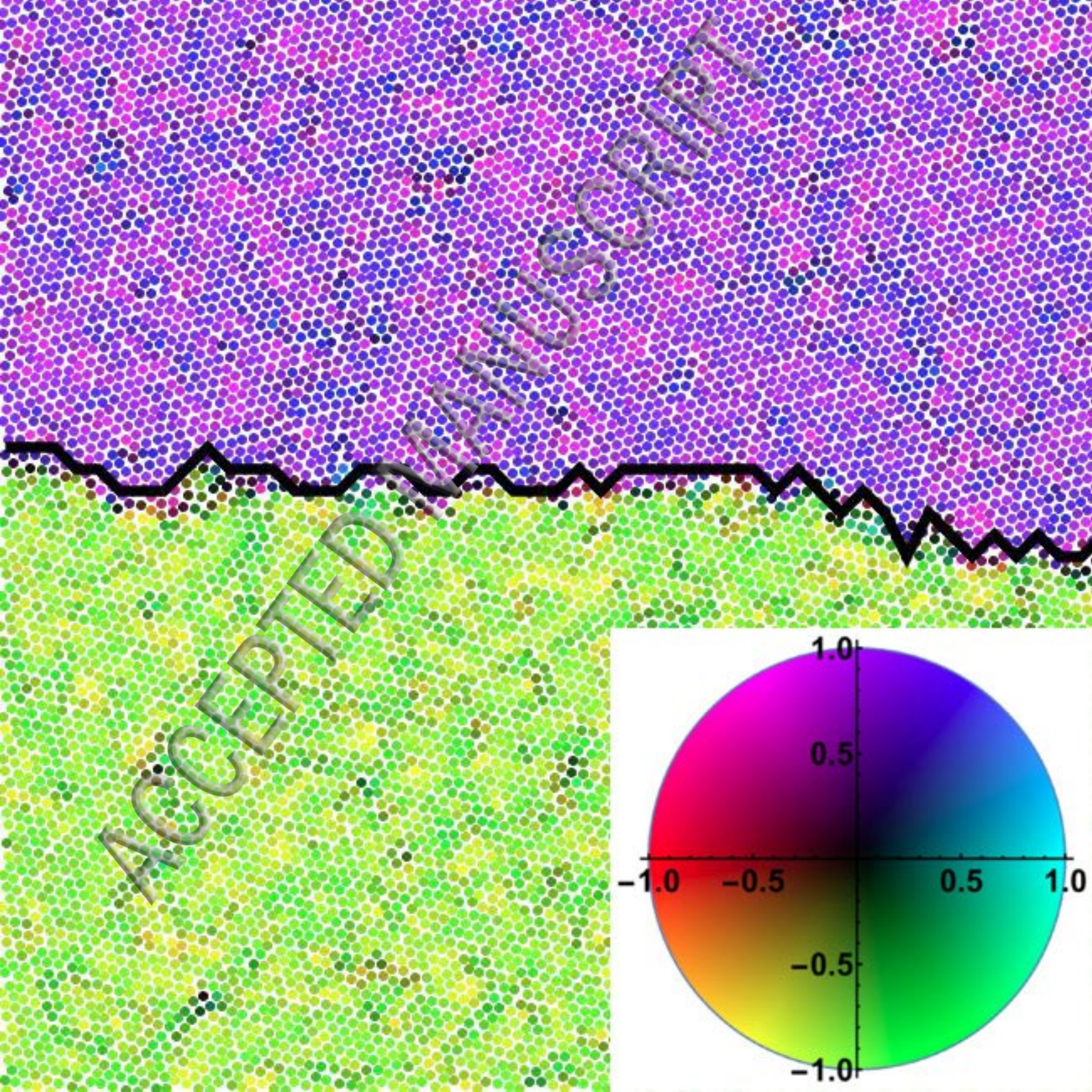

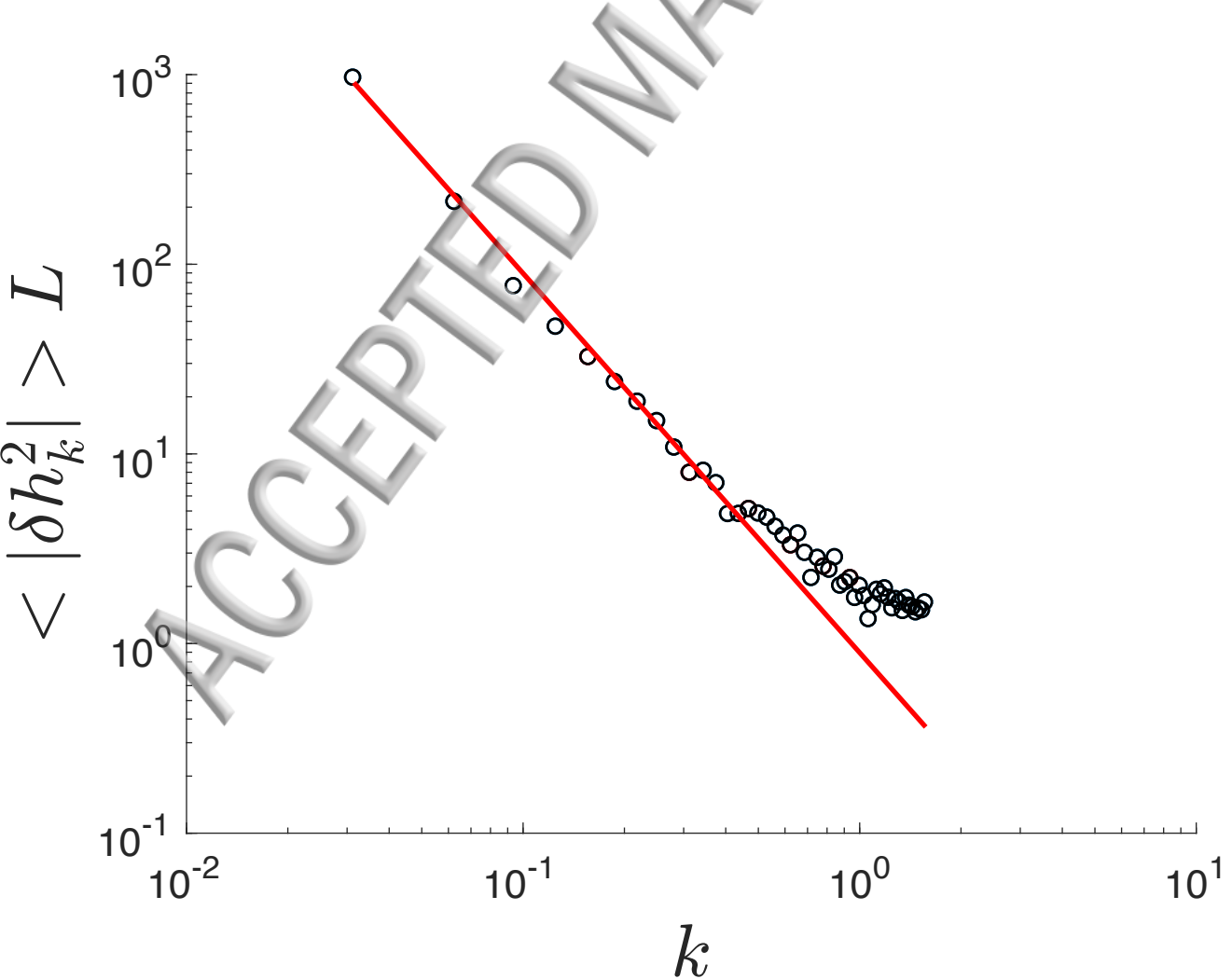

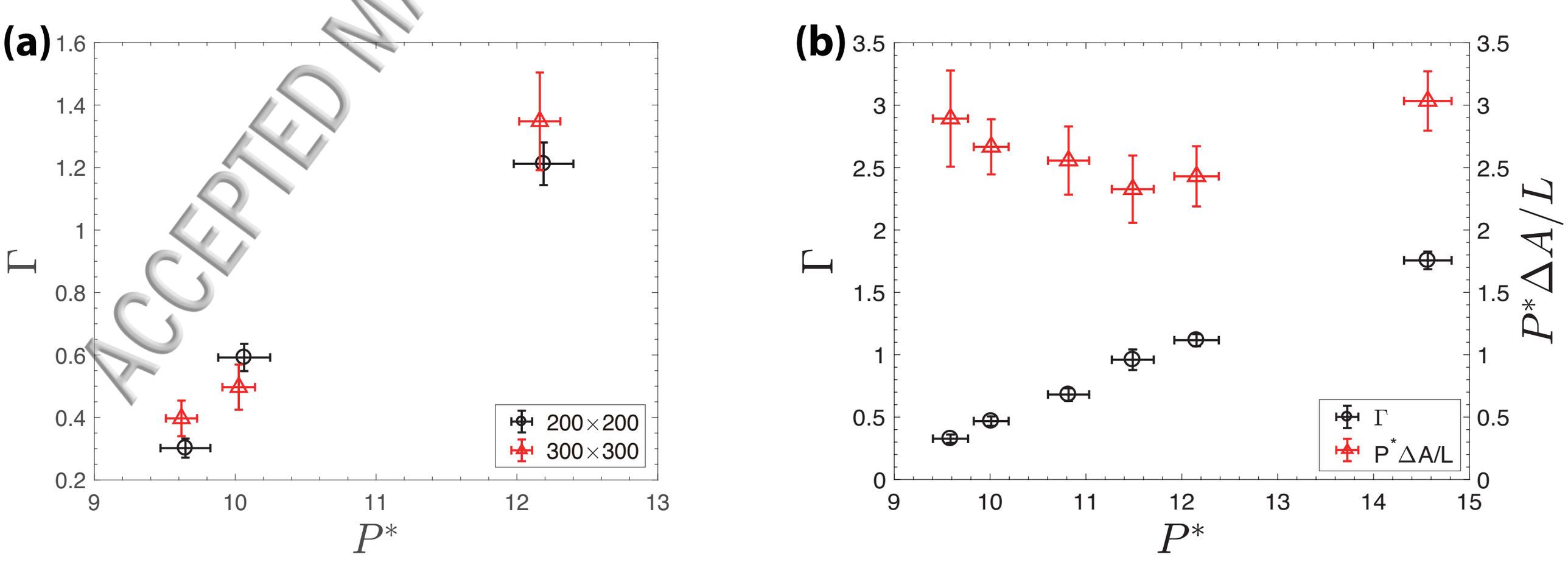

(a)

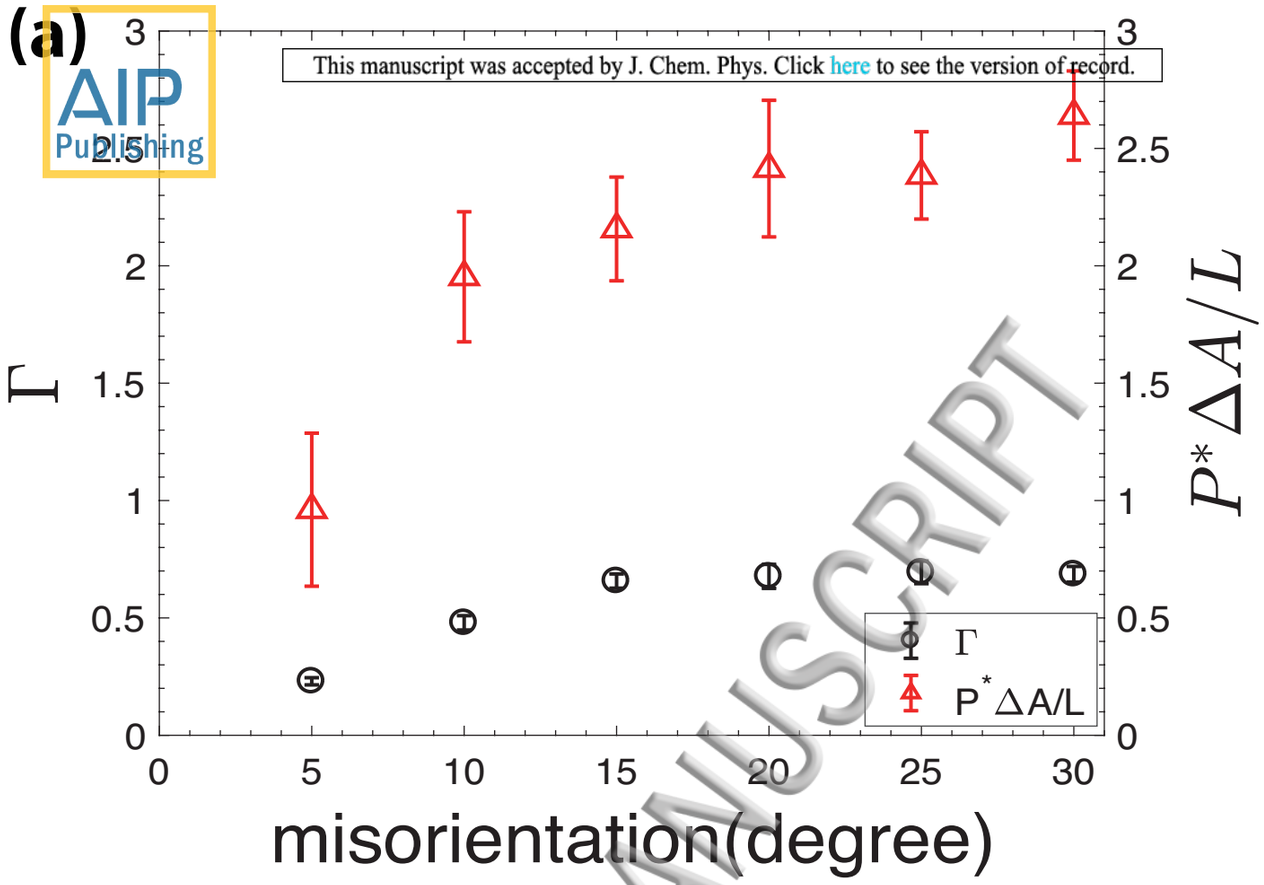


(b)

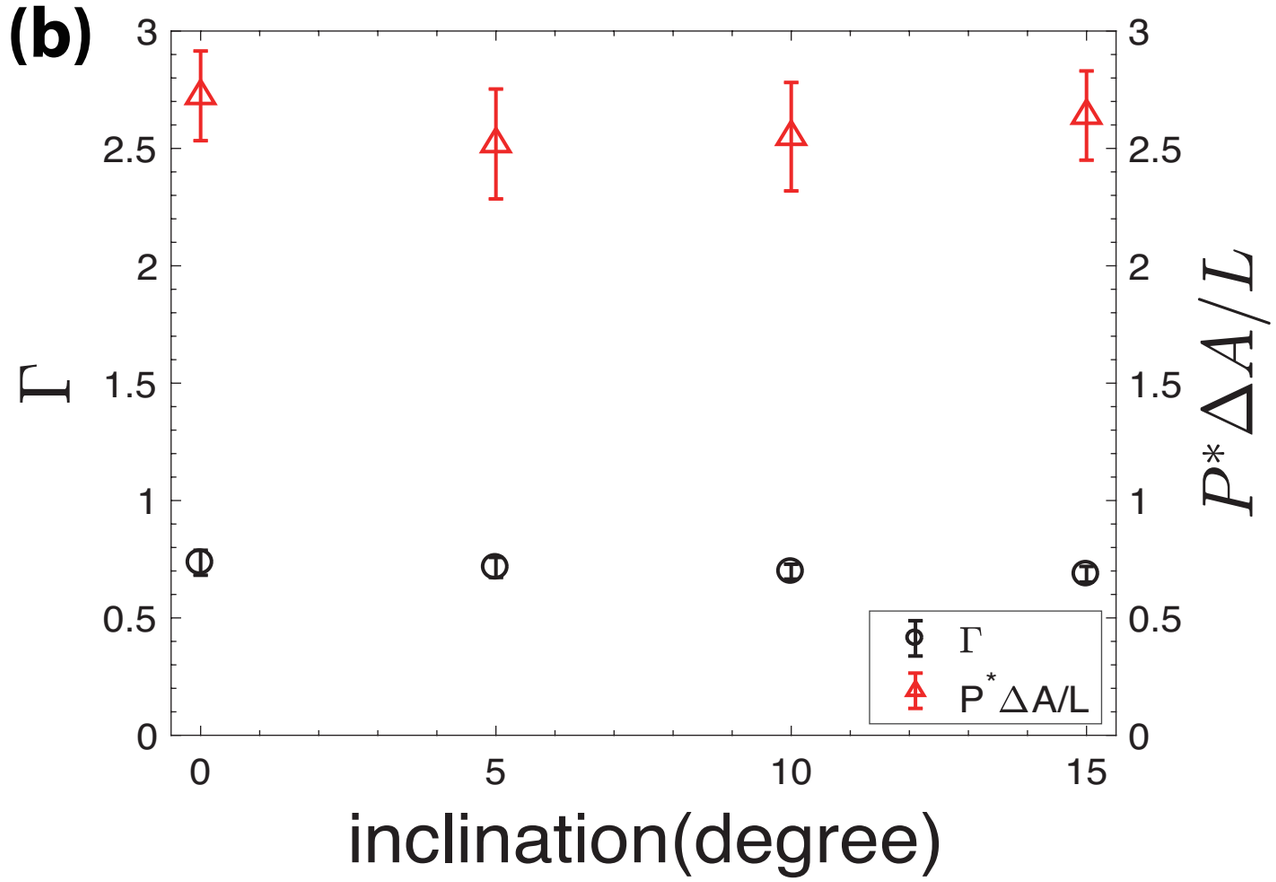


(c)

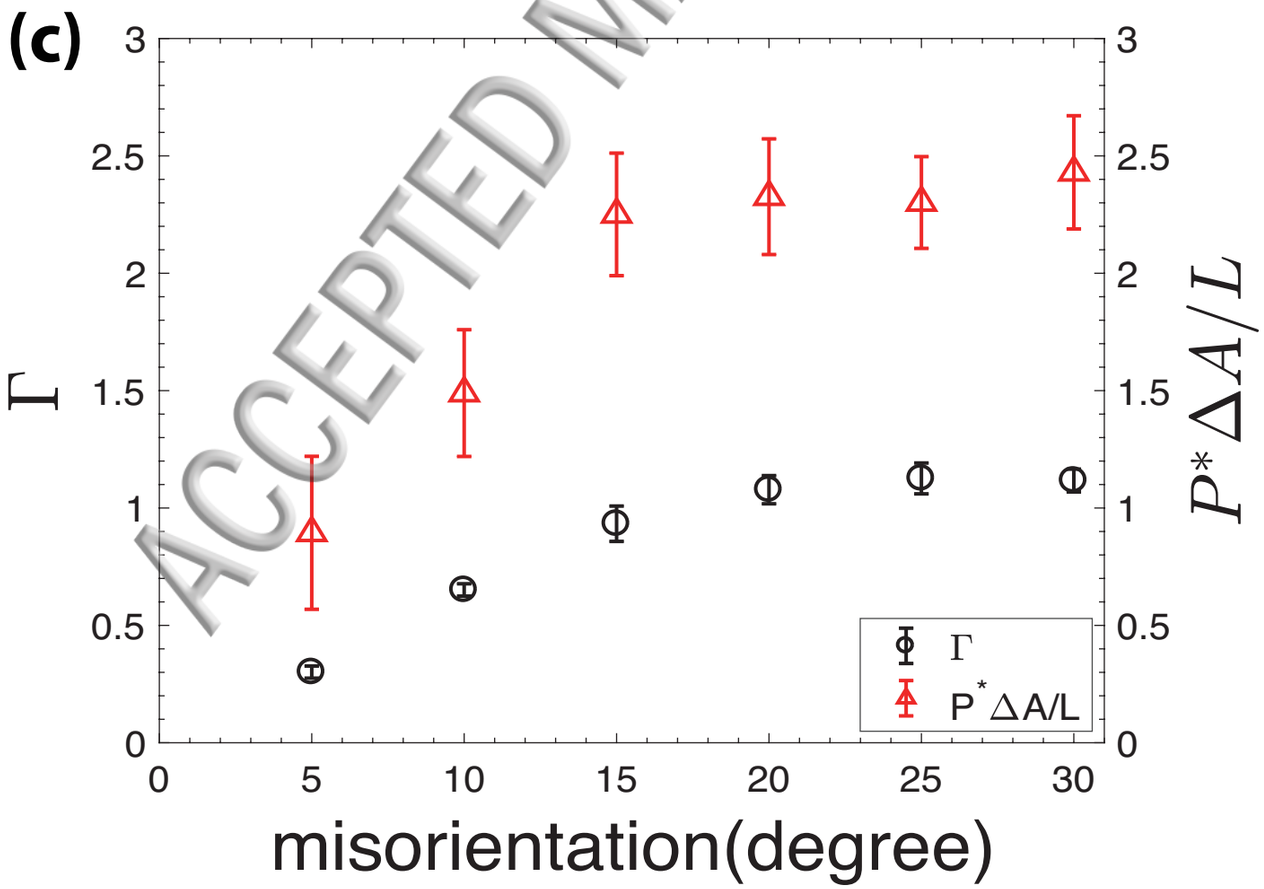


(d)